

Article

# Factors Affecting Tufa Degradation in Jiuzhaigou National Nature Reserve, Sichuan, China

Lixia Liu

Department of Environment, College of Architecture and Environment, Sichuan University, Chengdu 610065, China; lxliu2012@163.com; Tel.: +86-28-85407049

Received: 21 July 2017; Accepted: 12 September 2017; Published: 14 September 2017

**Abstract:** Water and tufa samples were collected from Arrow Bamboo Lake, the stream from Panda Lake to Five-Color Lake, Pearl Shoal and Shuzheng Lakes in Jiuzhaigou National Nature Reserve, China, between October 2013 and September 2014, to investigate tufa growth rate and water environment (water temperature, pH, electric conductivity, major ions and nutrients), and analyzed to explore the main causes of tufa degradation. The mean annual rate of tufa growth was low and varied within lakes, with the maximum deposit thickness of 332  $\mu\text{m}/\text{y}$ . The calcite saturation index ranged from 0.65 to 0.83. Scanning electron microscope images showed that the tufa deposits had non-isopachous structures, and diatoms were the dominant microorganisms that participated in tufa deposition. Porous and crystalline structures of deposits were linked with a high tufa growth and small amounts of diatoms. Conversely, tufa deposits with amorphous and loose structures showed a low crystal growth rate and a high number of diatoms. A one-way analysis of variance and a least significant difference test were applied to identify site differences in water chemistry. Linear correlations indicated that nitrate, phosphate and sulfate inhibit tufa growth ( $p < 0.05$ ). Increased nitrogen and phosphorus concentrations that originate mainly from atmospheric pollution and tourist activities at scenic attractions could trigger excessive diatom growth, which inhibits tufa precipitation. A series of measures should be implemented (e.g., the visitor number and vehicles should be regulated and controlled) to minimize tufa degradation in the Jiuzhaigou National Nature Reserve.

**Keywords:** tufa; aquatic environment; diatom; nutrient; statistical analysis; one-way ANOVA; tourist attraction

## 1. Introduction

Tufa is a localized precipitation of calcium carbonate ( $\text{CaCO}_3$ ) that is generated by rivers, lakes or springs in karst areas through certain physical, chemical and biological actions. Tufa contains the remains of micro- and macro-phytes, invertebrates and bacteria [1]. Tufa is widespread globally [2], and in some areas, massive tufa deposits can spread from meters to kilometers and form picturesque tufa landscapes, such as tufa waterfalls, tufa-dammed lakes and cascades. These natural landscapes are popular tourist destinations [1], such as Jiuzhaigou National Nature Reserve and Huanglong Scenic and Historic Interest Area in China, Plitvice National Park in Croatia, Havasupai Canyon in the U.S. and Dunns River Falls in Jamaica. Because of the rapidly-expanding global tourist industry, these magnificent landscapes are facing unexpected problems. Splendid tufa landscapes are destroyed easily by human interference [3]. The surge in tourist numbers has led to water pollution and trampling on tufa in scenic spots, and increased pressure is expected in terms of the conservation of tufa landscapes [4].

In general, tufa formations are governed by a complex relationship between physical, chemical and biological factors [5].  $\text{CaCO}_3$  deposition in natural water is represented by the following reaction:



CaCO<sub>3</sub> precipitation contributes to tufa deposition. Tufa deposition is driven mainly by the release of large amounts of carbon dioxide (CO<sub>2</sub>) from water to the atmosphere [6]. CO<sub>2</sub> removal is attributed to turbulence, mixing of water of different contents and the metabolic uptake of CO<sub>2</sub> by photosynthetic organisms (e.g., plants, algae and mosses) [7]. Organisms facilitate or retard CaCO<sub>3</sub> formation [8–10]. This role can also be divided into physical and chemical effects [6]. Organisms can aid tufa deposition by trapping and binding CaCO<sub>3</sub> particles [11] and precipitating some CaCO<sub>3</sub> through photosynthesis by absorbing CO<sub>2</sub> from water [4]. Other metabolic types produce organic acids, which accelerate CaCO<sub>3</sub> dissolution [12]. Diatoms are an especially important group of algae that are distributed widely in aquatic ecosystems and are important in promoting the formation and dissolution of tufa [13].

CaCO<sub>3</sub> precipitation is endothermic, and tufa formation is accelerated with an increase in water temperature. The solubility of CaCO<sub>3</sub> and CO<sub>2</sub> decreases with increasing water temperature [14]. However, in turbulent waters, the principal cause of tufa deposition is CO<sub>2</sub> degassing, whereas the photosynthetic uptake of CO<sub>2</sub> and temperature effects are negligible [15,16].

All ions except for Ca<sup>2+</sup> and HCO<sub>3</sub><sup>−</sup> are extrinsic in water. Other research suggests that the presence of complexing ions (e.g., SO<sub>4</sub><sup>2−</sup>, Mg<sup>2+</sup>) and acidic organic molecules will reduce the concentrations of Ca<sup>2+</sup> and CO<sub>3</sub><sup>2−</sup> through ion pairing, which retards CaCO<sub>3</sub> deposition [10]. Several studies also have proven that PO<sub>4</sub><sup>3−</sup>, Mg<sup>2+</sup> and organic ligands inhibit tufa deposition by occupying the position of Ca<sup>2+</sup> in the lattice and by changing the crystal forms [17–19]. This explains why some streams are calcite supersaturated, but tufa deposition does not occur [6,18].

Jiuzhaigou National Nature Reserve (hereafter Jiuzhaigou) is a celebrated tourist attraction in China, and its unique water and tufa landscapes attract millions of visitors every year. Tourism has expanded gradually worldwide, and the number of tourists in Jiuzhaigou has increased from 27,000 in 1984 [20] to 5.1 million in 2015, which represents a 188-fold increase. Since the 1990s, excessive algal growth and tufa degradation have been observed in Jiuzhaigou [6,21]. A series of measures has been implemented within the reserve by the Jiuzhaigou Administrative Bureau, such as building pedestrian roads, banning logging, prohibiting farming and grazing and demolishing hotels and restaurants. However, tufa degradation and water pollution have continued.

A team from Jiuzhaigou International Laboratory for Ecology, Environment and Sustainability of Sichuan University researched tufa landscape changes [22], lacustrine deposits [23,24], forest succession [25], tourism [21,26] and air pollution [20,27,28] in Jiuzhaigou. Relatively little is known about the rate of tufa accumulation and the tufa deposit structure in particular environments. The complex relationships between the aquatic environment and tufa deposition are poorly understood. We hypothesize that water eutrophication facilitates excessive algae growth. These algae will participate in tufa deposition and form loose deposits that can be displaced easily by water.

The objectives of this study are: (1) to observe tufa deposit structures and to estimate the annual tufa deposition growth rate at selected sites, (2) to elucidate the relationship between tufa deposition and water environmental variables and (3) to explore the roles of diatoms in tufa deposition and the main causes of tufa degradation.

## 2. Materials and Methods

### 2.1. Study Area

Jiuzhaigou is located on the eastern fringe of the Qinghai-Tibet Plateau, in Jiuzhaigou County, Aba Tibetan, and Qiang Autonomous Prefecture, Sichuan, southwestern China. It is situated between 32°53′ and 33°20′ N and 103°46′ and 104°05′ E (Figure 1a). Jiuzhaigou is a watershed that consists of three main valleys, namely the Rize, Zezhawa and Shuzheng valleys (Figure 1b). Water flows from the south to the north.

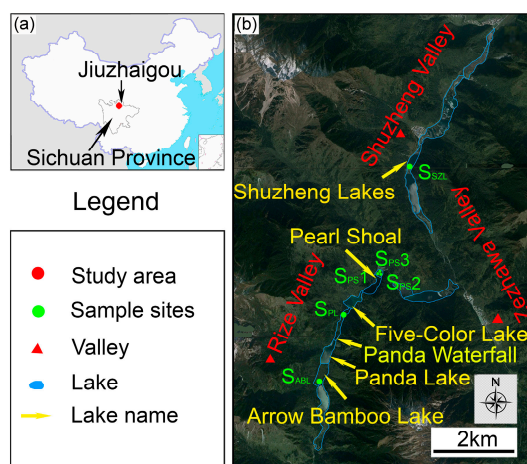


**Figure 1.** Maps showing: (a) The location of Jiuzhaigou; (b) The positions of the main tufa-depositing lakes and the approximate installation point of each substrate.

Four distinct seasons exist in Jiuzhaigou, i.e., dry spring and winter, wet summer and autumn. Based on meteorological data collected at Nuorilang of Jiuzhaigou, the mean annual precipitation is ~680 mm, with the majority of rainfall occurring between May and September. Precipitation is the main water source for lakes and rivers in the watershed. A large seasonal range occurs in mean monthly temperatures, from  $-4.0\text{ }^{\circ}\text{C}$  in January (in winter) to  $16.4\text{ }^{\circ}\text{C}$  in July (in summer). The mean annual temperature is  $6.8\text{ }^{\circ}\text{C}$ .

Jiuzhaigou's topography is complicated. The elevation ranges from 1996 m to 4764 m, with an average elevation of 2768 m above sea level [29]. Tufa is concentrated in the Rize and Shuzheng valleys, and the tufa deposits cover approximately  $2.4\text{ km}^2$ . However, in recent years, excessive algae growing and tufa degradation have been observed in Jiuzhaigou (Figure 2).



**Figure 2.** The changes of water and tufa landscape in Jiuzhaigou showing: (a) Algae growing; (b) Tufa landscape collapse.

## 2.2. Sampling

The experimental period was divided into the dry season (including October, November, December 2013 and March, April 2014) and wet season (including May, June, July, August and September 2014) according to monthly rainfall in the region. Ten field surveys were conducted monthly from October 2013 to September 2014 at six sites: Arrow Bamboo Lake ( $S_{ABL}$ ), the stream from Panda Lake to Five-Color Lake ( $S_{PL}$ ), Pearl Shoal ( $S_{PS1}$ ,  $S_{PS2}$  and  $S_{PS3}$ ) and Shuzheng Lakes ( $S_{SZL}$ ). Samples were collected at three sites on Pearl Shoal because this is a celebrated spot in Jiuzhaigou. Samples (500 mL) were collected near the surface (~0.10-m depth) and kept frozen in high-density polyethylene bottles, then transported to a laboratory in Chengdu within three days after collection for analyses. Before sampling, the water temperature (WT), pH and electric conductivity (EC) were

measured at each site with a portable multi-parameter probe (Multi 3420, WTW, Munich, Germany). Samples were analyzed in the laboratory for  $\text{Ca}^{2+}$ ,  $\text{Mg}^{2+}$ ,  $\text{K}^+$ ,  $\text{Na}^+$ ,  $\text{HCO}_3^-$ ,  $\text{SO}_4^{2-}$ ,  $\text{NO}_3^-$ ,  $\text{Cl}^-$ ,  $\text{F}^-$  and dissolved phosphorus (DP). Water samples (60 mL) for  $\text{Ca}^{2+}$ ,  $\text{Mg}^{2+}$ ,  $\text{K}^+$ ,  $\text{Na}^+$ ,  $\text{SO}_4^{2-}$ ,  $\text{NO}_3^-$ ,  $\text{Cl}^-$  and  $\text{F}^-$  analyses were filtered through 0.22- $\mu\text{m}$  sieves and were analyzed by using an ion chromatograph (ICS-900, Dionex, Sunnyvale, CA, USA). Dissolved phosphorus (25-mL subsample) and  $\text{HCO}_3^-$  (50-mL subsample) concentrations were determined with an ultraviolet-visible spectrophotometer (UV-2350, Unico, Shanghai, China) and by using 0.025 M hydrochloric acid (50 mL acid burette, Sichuan Shu Bo (Group) Co., Ltd., Chengdu, China), respectively.

Tufa deposition was monitored at the six sites from October 2013 to September 2014. Two rectangular Plexiglas substrates of 5 cm  $\times$  5 cm  $\times$  0.2 cm were mounted at each site in October 2013. A 6-mm hole was used to secure each substrate in a stream using a 25 to 30 cm-long stainless-steel screw [30]. The top and bottom faces of the substrates were oriented parallel to the water flow and were immersed in water as far as possible (Figure 3). Substrates were retrieved and packed for laboratory examination in October 2014. Small portions of tufa that had been deposited on each substrate were cut for scanning electron microscope (SEM) observation. The energy dispersive spectrum (EDS) analysis was performed to study the chemical composition of tufa deposits. The sampled tufa was coated with gold. Observations were performed with a scanning electron microscope (S-4800, Hitachi, Tokyo, Japan) at an accelerating voltage of 5 kV. X-ray diffraction (XRD) analysis was used to identify petrographic characteristics of tufa deposits through an X-ray diffractometer (XRD-6100, Shimadzu, Beijing, China). Diatoms in tufa deposits were identified using SEM images. Substrates mounted for tufa deposition in the red circle represent  $S_{P53}$  in Pearl Shoal.



**Figure 3.** Photograph at one of the studied sites.

### 2.3. Data Analysis

$\text{CaCO}_3$  precipitation is a function of  $\text{CO}_3^{2-}$  alkalinity and the availability of free  $\text{Ca}^{2+}$ , and these are combined in the saturation index. A calcite saturation index ( $SIc$ ) is applied as a measure of equilibrium. If the  $SIc$  exceeds 0,  $\text{CaCO}_3$  tends to deposit; otherwise,  $\text{CaCO}_3$  dissolves. The saturation index is defined using:

$$SIc = \log\left(\frac{IAP}{K}\right) \quad (2)$$

where  $IAP$  denotes an ion activity product (i.e.,  $\{\text{Ca}^{2+}\} \times \{\text{CO}_3^{2-}\}$ ) and  $K$  is the solubility product of the corresponding mineral [31].  $SIc$  was calculated by using the hydrogeochemistry simulation software Phreeqc3 from the U.S. Geological Survey using pH, water temperature, electric conductivity and ionic concentration.

Raw datasets for tufa deposition and water environmental measurements were normalized, and a one-way analysis of variance (one-way ANOVA) and a least significant difference test were applied to identify site differences in water chemistry and tufa growth. The interrelationships between different parameters were supported by linear correlation. All statistical analyses were performed using SPSS 19.0.

### 3. Results and Discussion

#### 3.1. Tufa Deposited on Substrates and Its Rate of Growth

Most substrates were covered with deposits. The water level changed at the studied sites except for Arrow Bamboo Lake ( $S_{ABL}$ ) and Shuzheng Lakes ( $S_{SZL}$ ), and it decreased in response to a decrease in precipitation between November 2013 and April 2014. During this period, substrates at four sites (i.e.,  $S_{PL}$ ,  $S_{PS1}$ ,  $S_{PS2}$  and  $S_{PS3}$ ) became exposed, and tufa growth on their surface stopped. Nevertheless, the thickness of the deposits at sites  $S_{PS1}$  and  $S_{PS3}$  were higher than  $S_{PS2}$  to some extent, and the diatoms were the major part of the deposited layer at  $S_{PS1}$  and  $S_{PS3}$ . Tourist season (from May to October) is the wet season in Jiuzhaigou, and tourist activities contributed to the increase in water nutrient levels of the  $S_{PS1}$  site located under the walkway, which promoted excessive diatoms participating in tufa deposits. For the  $S_{PS3}$  site, there were plentiful mosses. The mosses cannot grow directly on the substrate or rock surface, and above all, they usually settle down by means of small amounts of soil and water [32]. Therefore, the mosses will grow and colonize with the aid of algal mats at the  $S_{PS3}$  site at first, and then, a combination mats of algae and mosses will be formed gradually to control the tufa deposition. In that case, large amounts of algae appeared in the tufa deposits at the  $S_{PS1}$  and  $S_{PS3}$  sites and formed thicker sediments.

The differences in the components of deposits on the substrates were noticeable between the studied sites. The tufa deposition rate can be calculated from the tufa mass increments [14]. SEM observations revealed diatoms as the main organisms that participated in tufa deposition. The research also indicated that the species of diatoms have a distinct advantage in the water of Jiuzhaigou [33]. Tufa was deposited unevenly on each substrate at maximum and minimum thicknesses of 332  $\mu\text{m}/\text{y}$  ( $S_{PL}$ ) and 75  $\mu\text{m}/\text{y}$  ( $S_{SZL}$ ), respectively (Figure 4). Foreign diatoms were included in the tufa mass, and hence, the tufa mass that was used to calculate the deposition rate was overestimated somewhat.

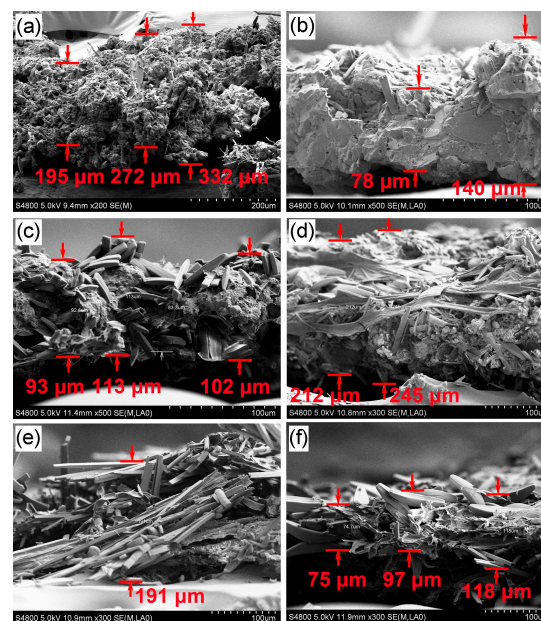


**Figure 4.** Deposit thickness under SEM at studied site  $s$  in one-year period. (a) Porous tufa deposits with uneven thicknesses (195 to 332  $\mu\text{m}/\text{y}$ ),  $S_{PL}$ ; (b) Compacted and clotted deposits (78 to 140- $\mu\text{m}$  thick),  $S_{PS2}$ ; (c) Loose deposits with asymmetrical thickness (93 to 113  $\mu\text{m}/\text{y}$ ) and abundant diatoms,  $S_{PS1}$ ; (d) Diatoms that cover non-isopachous deposits and form a network structure,  $S_{PS3}$ ; (e) The diatomaceous materials cover the deposits completely,  $S_{ABL}$ ; (f) Loose deposits with uneven thickness and diatoms embedded randomly,  $S_{SZL}$ .

Values of water depth and velocity refer to the ranges of the means at each site from field investigations and [7].

The *Slc* is an important indicator of tufa depositing or not. If we take into account that  $\text{CaCO}_3$  deposition occurs when *Slc* is greater than zero, and for a higher *Slc* value, the  $\text{CaCO}_3$  deposition rate increases in water [14]. The *Slc* values differed significantly at the six sites (*t*-test,  $p < 0.05$ ) (Figure 5). The highest annual mean value of *Slc* (0.83) occurred at  $S_{PS2}$ , followed by  $S_{PL}$  (0.79), and the lowest (0.65) occurred at  $S_{SZL}$ . *Slc* values exceeded zero, and so, we infer that tufa deposition should be higher at  $S_{PS2}$  and  $S_{PL}$  than at  $S_{ABL}$ ,  $S_{PS1}$ ,  $S_{PS3}$  and  $S_{SZL}$ . This is likely related to hydrodynamic conditions at the sites. Tufa growth was more rapid at sites with a rapid water flow, such as at downstream waterfalls. Table 1 lists the characteristics of tufa depositional environments at the six sites.  $S_{PL}$  and  $S_{PS2}$  are located on the stream bed below the Panda Waterfall and in a depression on the Pearl Shoal with turbulent flow, respectively. High flow velocities and turbulence enhance  $\text{CO}_2$ , which favors  $\text{CaCO}_3$  precipitation at  $S_{PS2}$  and  $S_{PL}$  [6,15,34], and when the water velocity is greater than  $120 \text{ cm}\cdot\text{s}^{-1}$ , variations in water velocity will not cause  $\text{CaCO}_3$  deposition [7]. The faster the water flows, the higher  $\text{CaCO}_3$  precipitation is within the threshold value ( $120 \text{ cm}\cdot\text{s}^{-1}$ ) of flow velocity at  $S_{PS2}$  and  $S_{PL}$ . Therefore, fast flow below the hydrodynamic threshold probably was one cause of promoting the  $\text{CaCO}_3$  deposition besides the hydrochemical parameters and biological factors considered in the following sections of this article.

**Table 1.** Main characteristics of the tufa depositional environments.

Sites	Location	Subenvironment	Altitude (m)	Water Depth (cm)	Water Velocity ( $\text{cm}\cdot\text{s}^{-1}$ )	Tufa Characteristics
$S_{ABL}$	Over Arrow Bamboo waterfalls, near walkway, close to road.	Areas of very low slope, stable groundwater recharge and paludification; the annual variation of water level was small.	2618	10–50	20–75	Loose sediment formed of algae and amorphous detritus, coated diatoms.
$S_{PL}$	100 m downstream from Panda Waterfall.	Turbulent water flow, steep slope, surface water recharge; water flow showed dramatic reduction due to seasonal decline in rainfall (from November 2013 to April 2014).	2507	0–50	90–225	Spongy tufa, diatoms involvement in deposits, well-formed rhombohedra of calcite crystals.
$S_{PS1}$	Under walkway, near entrance.	Areas of gentle slope, plentiful algae; strong water flow in the wet season <sup>a</sup> ; weak flow in the dry season <sup>b</sup> .	2452	0–20	50–90	Diatoms were the main part of loose sediment, finer spherulitic calcites.
$S_{PS2}$	In a depression of the central shoal.	Areas of shoal, including steeper slope, turbulent flow; the annual change of water flow was obvious.	2433	0–30	30–100	Diatoms participating in porous carbonate deposits, sheet-like calcite crystals.
$S_{PS3}$	Central shoal	Gentle slope with bryophytes growth; the annual variation of water flow was obvious.	2438	0–20	50–90	Large amounts of diatoms embedded in loose deposits, clumps of calcite crystals.
$S_{SZL}$	Opposite Shuzheng Mill, intersection of walkways.	Areas with gentle to nil slope stretching along the river bed; algae-rich, constant water flow.	2250	~100	0–50	Diatoms covered the loose deposits; scarce or absent carbonate deposits, poor calcites.

Notes: <sup>a</sup> Wet season, May to October. <sup>b</sup> Dry season, November to April.

Error bars represent the standard error of the mean. Different lowercase letters indicate significant differences ( $p < 0.05$ ) between different sites.

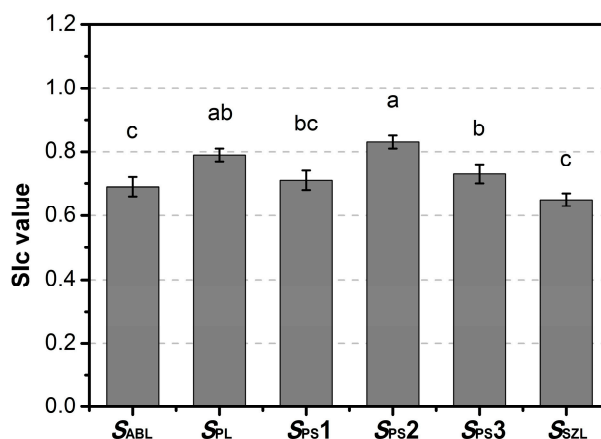


Figure 5. Spatial variations in the mean annual  $S_{Ic}$  values.

Calcite is the main component of tufa [7], and tufa in Jiuzhaigou is no exception. Three tufa samples were randomly selected for XRD (two samples) and EDS (one sample) analyses, respectively. Our results indicate that calcite is the main crystalline phase of tufa deposits (Figure S1a in Supplementary Materials), and tufa at Jiuzhaigou mainly contains chemical elements such as C (11.5%), O (49.9%), Si (1.3%) and Ca (37.3%) (Figure S1b). According to our quantitative analysis of the chemical composition,  $\text{CaCO}_3$  is the main component of the Jiuzhaigou tufa. Diatom colonies grow in random orientations that are interspersed within the tufa deposits. Because of competitive growth between diatoms and the initial direction of calcite crystal growth along the diatom stalk, the colonies formed uneven or non-isopachous sedimentary layers [14,35]. A higher  $S_{Ic}$  means a faster tufa growth. At sites with higher  $S_{Ic}$  values, the tufa deposit texture was compact and crystalline (Figure 4a,b), as observed at  $S_{PS2}$  and  $S_{PL}$ . Detritic carbonate and a higher amount of diatoms existed within the deposits at  $S_{PS1}$ ,  $S_{PS3}$ ,  $S_{ABL}$  and  $S_{SZL}$  (Figure 4c–f). A comparison between  $S_{Ic}$  and tufa deposition thickness does not indicate a simple relationship. A good example is the comparison of  $S_{PS2}$  and  $S_{PS3}$ . Although the highest annual mean value of  $S_{Ic}$  was 0.83 at  $S_{PS2}$ , the thickness of tufa growth ranged only from 78  $\mu\text{m}/\text{y}$  to 140  $\mu\text{m}/\text{y}$ . The  $S_{Ic}$  value at  $S_{PS3}$  was only 0.73, but the tufa deposits thickness varied between 212  $\mu\text{m}/\text{y}$  and 245  $\mu\text{m}/\text{y}$ . This discrepancy results from their different components and textures, which is reflected in the different proportions of diatoms in the deposits (Figure 4b,d).

### 3.2. Tufa Deposition and Hydrochemistry

Tufas are fed with  $\text{CO}_2$ -saturated water with a soil origin, and a healthy water environment is a prerequisite for tufa precipitation. Table S1 lists the characteristics of the major hydrochemical parameters at six sites during the study period.  $\text{Ca}^{2+}$  (49.84–60.16  $\text{mg}\cdot\text{L}^{-1}$ ) and  $\text{HCO}_3^-$  (189.58–248.77  $\text{mg}\cdot\text{L}^{-1}$ ) were the dominant cation and anion, respectively.  $\text{Mg}^{2+}$  (12.30–13.70  $\text{mg}\cdot\text{L}^{-1}$ ) and  $\text{SO}_4^{2-}$  (20.69–22.73  $\text{mg}\cdot\text{L}^{-1}$ ) were the second-most-abundant cation and anion, respectively. Except for water temperature and  $\text{SO}_4^{2-}$ , significant differences emerged in other hydrochemical measurements, including pH,  $\text{Ca}^{2+}$ ,  $\text{Mg}^{2+}$ ,  $\text{HCO}_3^-$ ,  $\text{NO}_3^-$ , and DP between the six studied sites at a  $p < 0.05$  level (Table 2). The pH differed between sites ( $F = 4.518$ ,  $p < 0.01$ ), with the highest (8.35) and lowest value (8.16) occurring at  $S_{PS2}$  and  $S_{ABL}$ , respectively. Differences in  $\text{NO}_3^-$  ( $F = 5.024$ ,  $p < 0.01$ ) and DP concentrations ( $F = 2.672$ ,  $p < 0.05$ ) were also significant between sites.  $\text{SO}_4^{2-}$  concentrations ( $p = 0.756$ ) and water temperature ( $p = 0.520$ ) were insignificantly different between different sites.  $\text{Ca}^{2+}$  concentrations decreased gradually in water samples that were collected along the water flow direction. A similar decreasing pattern was also observed in  $\text{HCO}_3^-$ . Such chemical changes likely result from  $\text{CaCO}_3$  deposition. The  $\text{NO}_3^-$  concentrations increased with water flow (from 0.73  $\text{mg}\cdot\text{L}^{-1}$  to 1.11  $\text{mg}\cdot\text{L}^{-1}$ ), and this may be interpreted as a consequence of nutrient accumulation in the streams. The highest concentrations of  $\text{Ca}^{2+}$ ,  $\text{HCO}_3^-$  and DP appeared at the  $S_{ABL}$  site, and a maximum  $\text{NO}_3^-$

concentration was observed at  $S_{SZL}$ .  $\text{NO}_3^-$  and DP concentration minima were observed at  $S_{PL}$ , whereas minimum contents of  $\text{Ca}^{2+}$  and  $\text{HCO}_3^-$  emerged at  $S_{SZL}$ . A higher tufa deposition rate occurred at  $S_{PS2}$  and  $S_{PL}$ , and a lower tufa deposition rate occurred at  $S_{ABL}$  and  $S_{SZL}$ . It is likely that these result from low nutrient levels and moderate concentrations of  $\text{Ca}^{2+}$  and  $\text{HCO}_3^-$ , which are most suitable for tufa growth [36].

**Table 2.** Hydrochemistry measurements at the studied sites.

Site *	$S_{ABL}$	$S_{PL}$	$S_{PS1}$	$S_{PS2}$	$S_{PS3}$	$S_{SZL}$	<i>F</i>	<i>p</i>
Water temp (°C)	7.69 (0.94)	8.35 (0.88)	7.69 (0.55)	8.44 (0.57)	8.90 (0.43)	9.64 (0.83)	0.851	0.520
pH	8.16 (0.04) <sup>b</sup>	8.34 (0.14) <sup>a</sup>	8.23 (0.03) <sup>ab</sup>	8.35 (0.02) <sup>a</sup>	8.28 (0.04) <sup>ab</sup>	8.28 (0.02) <sup>ab</sup>	4.518	0.002
$\text{Ca}^{2+}$ (mg·L <sup>-1</sup> )	60.16 (3.21) <sup>a</sup>	55.14 (1.57) <sup>ab</sup>	56.78 (2.01) <sup>ab</sup>	55.60 (1.78) <sup>ab</sup>	54.85 (2.54) <sup>ab</sup>	49.84 (0.54) <sup>b</sup>	2.423	0.047
$\text{Mg}^{2+}$ (mg·L <sup>-1</sup> )	13.02 (0.42) <sup>ab</sup>	12.30 (0.25) <sup>b</sup>	13.63 (0.25) <sup>a</sup>	13.53 (0.29) <sup>a</sup>	13.54 (0.26) <sup>a</sup>	13.70 (0.21) <sup>a</sup>	3.049	0.017
$\text{HCO}_3^-$ (mg·L <sup>-1</sup> )	248.77 (9.69) <sup>a</sup>	202.51 (3.70) <sup>c</sup>	224.95 (3.78) <sup>b</sup>	223.53 (3.87) <sup>b</sup>	220.06 (2.96) <sup>b</sup>	189.58 (3.26) <sup>c</sup>	15.6	0.001
$\text{SO}_4^{2-}$ (mg·L <sup>-1</sup> )	21.57 (1.30)	20.69 (1.06)	22.37 (0.63)	21.77 (0.86)	21.87 (0.82)	22.73 (0.79)	0.526	0.756
$\text{NO}_3^-$ (mg·L <sup>-1</sup> )	0.90 (0.06) <sup>ab</sup>	0.73 (0.13) <sup>b</sup>	1.09 (0.04) <sup>a</sup>	1.08 (0.05) <sup>a</sup>	1.08 (0.04) <sup>a</sup>	1.11 (0.06) <sup>a</sup>	5.024	0.001
(DP) (mg·L <sup>-1</sup> )	0.009 (0.002) <sup>a</sup>	0.003 (0.001) <sup>b</sup>	0.004 (0.001) <sup>b</sup>	0.003 (0.001) <sup>b</sup>	0.004 (0.001) <sup>b</sup>	0.005 (0.001) <sup>ab</sup>	2.672	0.046

Notes: \*  $S_{ABL}$ , Arrow Bamboo Lake site;  $S_{PL}$ , stream from Panda Lake to Five-Color Lake;  $S_{PS1}$ ,  $S_{PS2}$ ,  $S_{PS3}$ , three sites in Pearl Shoal;  $S_{SZL}$ , Shuzheng Lakes site.

All values are expressed as the mean  $\pm$  the standard error of the mean; different lowercase letters in the same row indicate a significant difference ( $p < 0.05$ ).

Statistically-significant positive correlations existed between *S<sub>IC</sub>* and pH and  $\text{Ca}^{2+}$  and  $\text{HCO}_3^-$  ( $p < 0.05$ , Figure 6), which can be described by linear equations. In contrast, *S<sub>IC</sub>* had significant negative linear correlations with DP,  $\text{SO}_4^{2-}$  and  $\text{NO}_3^-$ , respectively ( $p < 0.05$ ). The relationships between *S<sub>IC</sub>* and pH and  $\text{NO}_3^-$  were significant ( $p < 0.01$ ). However, no apparent relationships existed between *S<sub>IC</sub>* and the water temperature ( $p = 0.146$ ) and  $\text{Mg}^{2+}$  ( $p = 0.761$ ).

The alkaline water environment favored  $\text{CaCO}_3$  deposition, and a high pH was associated with more intense tufa precipitation [37]. Therefore, at sites  $S_{PL}$  and  $S_{PS2}$ , rapid  $\text{CO}_2$  degassing in turbulent flow led to a pH increase, and tufa deposition was high, as mentioned above. Certain elemental changes could also affect tufa deposition. In addition to dominant  $\text{Ca}^{2+}$  (18% of the ionic concentration) and  $\text{HCO}_3^-$  (70% of the ionic concentration),  $\text{Mg}^{2+}$  and  $\text{SO}_4^{2-}$  were the next dominant anions (4.5% and 7.0% of the ionic concentration, respectively) in water. The material source of tufa deposition is suggested to be from  $\text{Ca}^{2+}$  and  $\text{HCO}_3^-$ , and higher  $\text{Ca}^{2+}$  and  $\text{HCO}_3^-$  concentrations yield a higher tufa growth rate, with all other conditions being the same in the parent water [38]. Some studies also showed that a  $\text{SO}_4^{2-}$  reduction increased the *S<sub>IC</sub>* and favored  $\text{CaCO}_3$  precipitation, and  $\text{Mg}^{2+}$  and  $\text{SO}_4^{2-}$  can reduce  $\text{Ca}^{2+}$  and  $\text{CO}_3^{2-}$  concentrations through ion pairing, which can inhibit  $\text{CaCO}_3$  deposition [10,39]. Moreover,  $\text{Mg}^{2+}$  can occupy the  $\text{Ca}^{2+}$  position in the lattice during tufa growth to inhibit  $\text{CaCO}_3$  deposition [17]. Nevertheless, the  $\text{Mg}^{2+}$  concentration that hinders  $\text{CaCO}_3$  deposition exceeds 240 mg L<sup>-1</sup> [2].  $\text{Mg}^{2+}$  in water originates mainly from carbonate (e.g., dolomites and marls) weathering and dissolution [40]. The  $\text{Mg}^{2+}$  concentration in the Jiuzhaigou surface water ranged from 11.0 mg·L<sup>-1</sup> to 15.0 mg·L<sup>-1</sup>, which is far below that required to inhibit tufa deposition. Our results indicate that the tufa growth rate appeared to have a negative correlation with  $\text{SO}_4^{2-}$ , whereas the correlation between tufa growth rate and  $\text{Mg}^{2+}$  was not significant ( $p > 0.05$ ). In this study, the  $\text{PO}_4^{3-}$  measurement is less than the threshold detection level (0.001 mg·L<sup>-1</sup>) of the instrument. DP exists mainly as phosphate in water. As the main form of phosphate, orthophosphate ( $\text{PO}_4^{3-}$ ) is also absorbed easily by algae in water [41]. Therefore, the differences in DP content mirror the  $\text{PO}_4^{3-}$  concentration change to some extent. Some research shows that  $\text{PO}_4^{3-}$  is adsorbed on the calcite surface, blocks active crystal-growth sites, inhibits calcite nucleation and “poisons” tufa deposition in water [19]. Our results are consistent with this report that suggests that a significant inverse correlation exists between the tufa deposition rate and the DP concentrations. Fossil-fuel (coal and oil) burning is one of the major sources of sulfate via atmospheric deposition into water. The increased nitric and

sulfuric acids in surface water from nitrogen and sulfur deposition would cause tufa degradation in Jiuzhaigou [42]. The tufa deposition rate was significantly negatively related to  $\text{NO}_3^-$ ,  $\text{SO}_4^{2-}$  and  $\text{PO}_4^{3-}$  contents in water, because changes in their concentrations caused hydrochemical property changes of water.

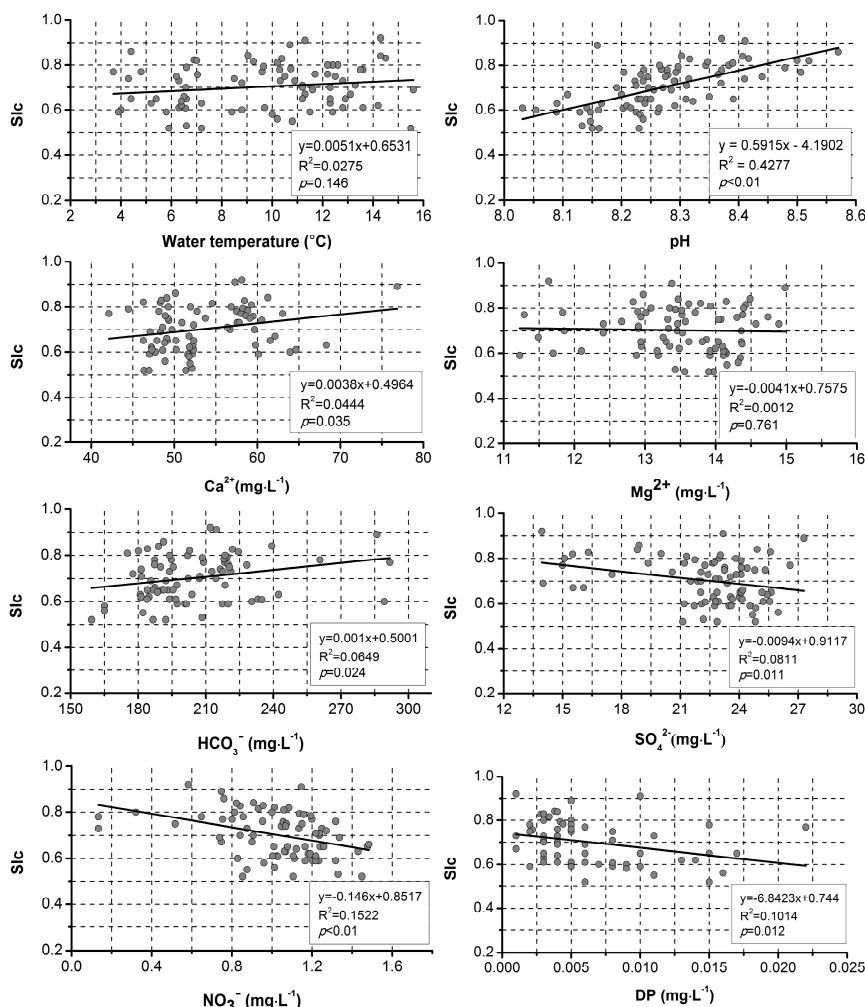


Figure 6. Linear fit between *S/c* and hydrochemical variables for the studied sites.

The aqueous  $\text{Ca}^{2+}$  concentration and *S/c* are good indicators of tufa deposition. Tufa deposition occurs mainly in water with a  $\text{Ca}^{2+}$  concentration that exceeds  $80 \text{ mg}\cdot\text{L}^{-1}$  [2], and with an *S/c* value that exceeds 0.80 [43,44].  $\text{Ca}^{2+}$  concentrations in Jiuzhaigou ranged from  $34.07 \text{ mg}\cdot\text{L}^{-1}$  to  $68.30 \text{ mg}\cdot\text{L}^{-1}$ , and the *S/c* values exceeded zero (0.52–0.91); however, the annual mean values were less than 0.80 at the studied sites except for  $S_{PS2}$  (0.83) (Figure 5), which does not favor tufa deposition.

### 3.3. Roles of Diatoms in Tufa Deposition

SEM observations indicated that abundant diatom flora existed in the deposits at the studied sites. These diatoms belong to different morphological groups and were composed mainly of *Synedra* (Figure 7a,b,d,e), *Fragilaria* (Figure 7c,d), *Navicula* (Figure 7c), *Cymbella* (Figure 7f) and *Melosira* (Figure 7e). Diatoms showed variable orientations in deposits over the substrates because of their competitive growth (Figures 4 and 7), and some diatoms produced mucilaginous secretions on the tufa surface (Figure 8a,d,e,f). The tufa deposits that were formed on the substrates during the experiment exhibited various structures. Some displayed clotted and honeycombed surfaces (Figure 7a,b), whereas

others showed loose and fragmented structures (Figure 7c,d) or surfaces that were covered completely with a diatom mat that was composed of interwoven stalks (Figure 7e,f).

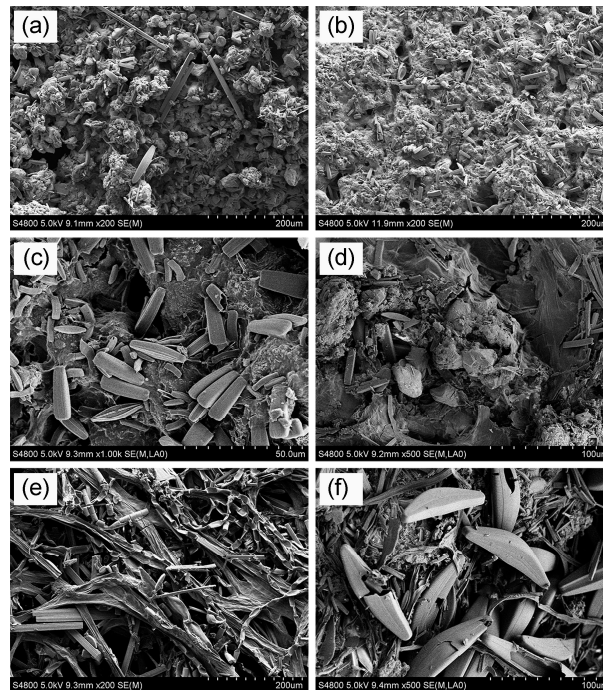


**Figure 7.** Scanning electron micrographs of tested samples showing superficial deposit characteristics. (a) Some diatoms on the porous tufa surface,  $S_{PL}$ ; (b) Porous calcareous deposit surface with diatoms,  $S_{PS2}$ ; (c) Diatoms of *Fragilaria* and *Navicula* on loose deposits,  $S_{PS1}$ ; (d) Diatoms (*Fragilaria*) embed in loose deposits,  $S_{PS3}$ ; (e) Dense growths of diatoms (*Fragilaria* and *Melosira*) produce a mat composed of interwoven stalks that cover the deposits completely,  $S_{ABL}$ ; (f) Diatom (*Cymbella*) communities cover the deposits fully,  $S_{SZL}$ .

As mentioned above, calcite crystals were common components of tufa that were formed during the experiment (Figures 8a–d and 9a–d). Crystals exhibited different sizes that ranged from less than 1  $\mu\text{m}$  to 50  $\mu\text{m}$ , and various shapes were arranged as hemispheres (Figure 8b,d), rhombs (Figures 8c and 9a), sheets (Figure 9b) and grains (Figures 8a and 9c,d). However, the finer  $\text{CaCO}_3$  crystals tended to have a detritic habit and were arranged in an amorphous pattern (Figure 9d,e,f). A higher magnification showed a number of irregular micropores (less than 1  $\mu\text{m}$  in diameter) on the rough surface of the calcite (Figure 8f). Some calcite crystals contained a central pore, and the pores were partially filled with diatom stalks (Figure 8b,d) or limestone (Figure 8c), which represents spaces where diatoms grew in situ, decayed rapidly and left hollow tubes [36,45,46]. Researchers summarized this phenomenon as diatom bioturbation (i.e., a micro-boring effect) [47,48].

Diatom communities could trap (Figure 8b), bind (Figure 8a) and bond calcite crystals (Figure 8e) as a result of their growth and certain metabolic activities (i.e., production of mucilaginous secretions that attach to the calcite surface) [47]. As mentioned in Section 3.2, the calcite growth rate depended on the hydrochemistry of the parent water. Our results indicate that diatoms were important in various tufa deposition structures. Research has shown that a high tufa growth rate favors a crystalline texture and that the tufa deposit with a porous or clotted structure is related to a high growth rate of calcite crystals [14]. The deposits at  $S_{PS2}$  and  $S_{PL}$  with higher tufa growth rates are good examples for such structures. In contrast, for a low tufa growth rate, loosely structured tufa and numerous diatoms were deposited. For instance, at  $S_{SZL}$ , with the lowest tufa deposition rate, tufa built of detritic materials and abundant diatoms formed.

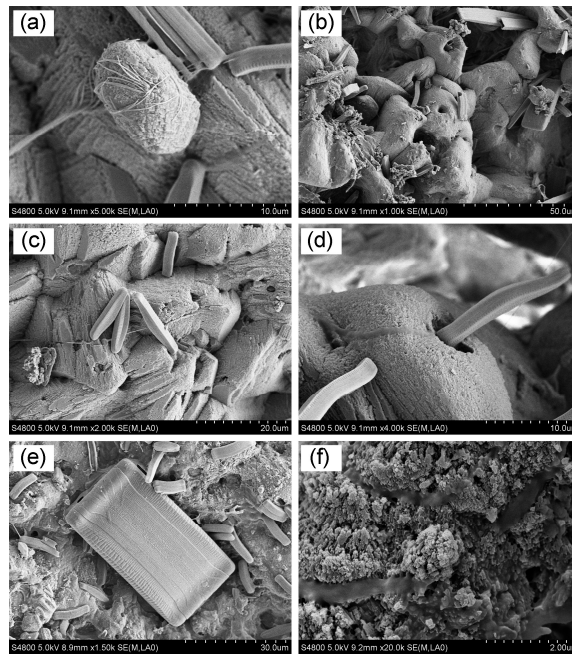


**Figure 8.** Scanning electron micrographs of secretions produced from diatoms and pores in tufa deposits. (a) Diatoms and their thread-like secretions that entwine  $\text{CaCO}_3$  particles,  $S_{PS1}$ ; (b,c) Common occurrence of pores in the center of calcite crystals and pores obstructed partially by decayed diatoms or limestone,  $S_{PL}$ ; (d) Calcite crystal engulfs part of one diatom stalk and mucilaginous secretions produced from diatoms,  $S_{PL}$ ; (e) Diatom flora of *Fragilaria* and their secretions on the tufa surface,  $S_{PS2}$ ; (f) A higher magnification view shows a rough and loose  $\text{CaCO}_3$  exterior and filamentous secretions,  $S_{PS3}$ .

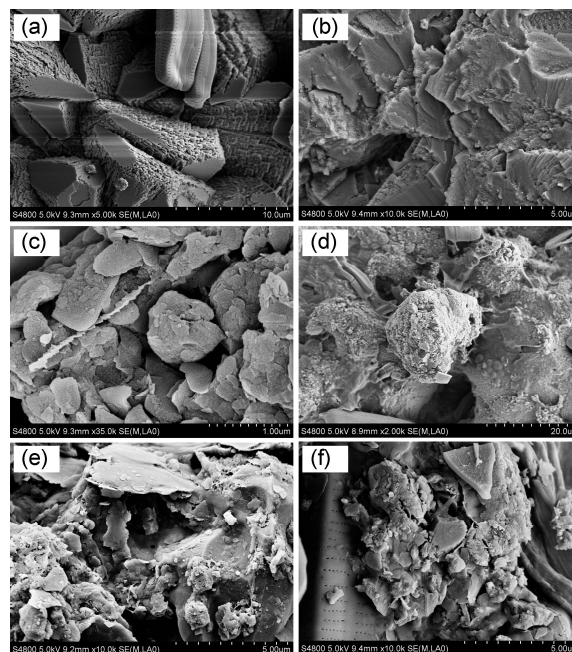


**Figure 9.** Scanning electron micrographs of  $\text{CaCO}_3$  crystals with various sizes and shapes. (a) Well-formed rhombohedra in a cluster of calcite crystals,  $S_{PL}$ ; (b) Sheet-like calcite crystals and their aggregates,  $S_{PS2}$ ; (c) Finer spherulitic aggregates of calcites,  $S_{PS1}$ ; (d) Clumps of calcite and aggregates,  $S_{PS3}$ ; (e) Amorphous detritus and aggregations,  $S_{ABL}$ ; (f) Detritic mineral grains and loose aggregations,  $S_{SZL}$ .

The occurrence of tufa deposition is caused mainly by CO<sub>2</sub> degassing from water. Algae can remove CO<sub>2</sub> by photosynthesis and drive CaCO<sub>3</sub> deposition. However, algae that favor tufa deposition via photosynthesis to absorb CO<sub>2</sub> occurred mainly in sluggish or quiescent water [13]. A large terrain variation exists in Jiuzhaigou, and water flows through multi-level waterfalls and ramps. CO<sub>2</sub> uptake by algal photosynthesis to aid tufa growth is negligible. However, algal metabolism can produce organic acids, which leads to a decrease in pH and CaCO<sub>3</sub> dissolution [12].

Low nutrient levels contribute to tufa formation [5], and our results in Section 3.2 showed that the tufa growth rate was significantly negatively related to NO<sub>3</sub><sup>-</sup> and PO<sub>4</sub><sup>3-</sup>. Trophic status and ion concentration are major drivers of diatom growth [49]. Diatoms are good bio-indicators of water nutrient enrichment [50,51]. Anthropogenic activities are major sources of phosphate and nitrate pollution in aquatic ecosystems. Besides fossil fuels, automobile exhaust emissions are also an important source of nitrate in water. Phosphorus gets into the water mainly through various sources including weathered soils from igneous rocks, domestic sewage containing human excrement, detergents in industrial waste and agricultural drainage [41]. Previous studies have suggested that nitrogen deposition from neighboring areas led to water eutrophication and excessive algal growth, and tourist activities have also resulted in an increase in nitrogen and phosphorus concentrations in the lakes of Jiuzhaigou [27,52]. Maximum concentrations of NO<sub>3</sub><sup>-</sup> and PO<sub>4</sub><sup>3-</sup> appeared at S<sub>SZL</sub> and S<sub>ABL</sub> with low tufa growth rates, loose deposited structures and a higher amount of diatoms. Conversely, minimum contents of NO<sub>3</sub><sup>-</sup> and PO<sub>4</sub><sup>3-</sup> existed at S<sub>PL</sub> with a higher tufa deposition rate, clotted deposits and a smaller number of diatoms. Shuzheng Lakes (S<sub>SZL</sub>) is located in the lower reaches of water flow of the six sites, and the high nutrient concentrations are likely to result from nutrient enrichment along the water flow. Arrow Bamboo Lake (S<sub>ABL</sub>) is an important visiting transit station for tourists, and frequent tourist activities contribute to an increase in water nutrient levels. High nutrient concentrations promote excessive diatom growth. Therefore, these diatoms participate in tufa deposition and form loose deposits with stability and erosion-resistance weakening.

In conclusion, besides industrial pollution from neighboring areas, automobile exhaust emissions may be an additional source of NO<sub>3</sub><sup>-</sup> in the surface water of Jiuzhaigou. With rapid developments in tourism, tourist activities result in obvious increases in nitrogen and phosphorus concentrations. Water eutrophication is likely a cause of concern for triggering tufa degradation in Jiuzhaigou. As tufa is so easily damaged by anthropogenic activities, specific measures, for example a strict control of the number of tourists, motor-vehicle management and emission standards should be established to alleviate future tufa degradation.

#### 4. Conclusions

The following conclusions can be made from this study:

- (1) During the study period, the average annual rate of tufa growth accompanied with algae deposition was low (75–332 μm/y), and significant differences resulted between selected sites in Jiuzhaigou.
- (2) Linear correlations showed that NO<sub>3</sub><sup>-</sup>, SO<sub>4</sub><sup>2-</sup> and PO<sub>4</sub><sup>3-</sup> were major factors in the aquatic environment that inhibited tufa deposition. Significant differences resulted in PO<sub>4</sub><sup>3-</sup> and NO<sub>3</sub><sup>-</sup> concentrations between sampled sites mainly because of tourist activity and nutrient enrichment in the water flow, as well as atmospheric precipitation, respectively.
- (3) Diatoms were associated frequently with tufa deposits. The deposits showed a non-isopachous characteristic because of the diatom's growing habit of a random growth orientation. Tufa deposits with porous and crystalline structures formed with high tufa growth. In contrast, for low crystal growth, tufa contained more diatoms, and a loose structure was deposited.
- (4) Anthropogenic activities, including industrial pollution, automobile exhaust emissions and tourist activities, contributed to an increase in nutrients in the water. Nutrient accumulation promotes excessive diatom growth, which contributes to a loose tufa deposit structure. The stability and erosion resistance of tufa deposits were weakened. Hence, abundant diatom growth is unfavorable to tufa deposition.

On the basis of the research results in this paper, some conclusions are obtained. A low tufa deposition rate exists at the six studied sites in Jiuzhaigou, because the  $\text{Ca}^{2+}$  concentrations and  $\text{SiC}$  values are low and because of diatom growth within the tufa deposits that results from the increased nutrient content in the water. Nevertheless, there are further fields yet to be revealed in the future work, which will undoubtedly shed considerable light on the dense investigations of the tufa deposit sampling, the research of the total microbial involvement in the calcite precipitation, as well as the effects of hydrodynamic conditions on the tufa deposition.

**Supplementary Materials:** The following are available online at [www.mdpi.com/2073-4441/9/9/702/s1](http://www.mdpi.com/2073-4441/9/9/702/s1), Figure S1: (a) X-ray diffraction (XRD) spectrogram and (b) Energy dispersive spectrum (EDS) diagram of tufa samples, Table S1: The major water parameters of the studied sites.

**Acknowledgments:** We would like to express our appreciation to the editors and anonymous reviewers for their useful comments on the earlier version of the manuscript. We also thank Jiuzhaigou Administrative Bureau for providing accommodation for this research.

**Conflicts of Interest:** The authors declare no conflict of interest.

## References

1. Ford, T.D.; Pedley, H.M. A review of tufa and travertine deposits of the world. *Earth Sci. Rev.* **1996**, *41*, 117–175. [[CrossRef](#)]
2. Pentecost, A. *Travertine*; Springer Netherlands: Dordrecht, The Netherlands, 2005.
3. Dramis, F.; Fubelli, G. Holocene stages of tufa deposition/erosion in Ethiopia: The role of climate fluctuations and human impact. In Proceedings of the EGU General Assembly Conference, Vienna, Austria, 27 April–2 May 2014; European Geosciences Union: Munich, Germany, 2014.
4. Pentecost, A.; Zhang, Z. A note on freshwater research in China, with some observations on the algae from Doupe Pool, Guizhou Province. *Freshw. Forum* **2001**, *15*, 77–84.
5. Jones, B.; Renaut, R.W. Calcareous Spring Deposits in Continental Settings. *Dev. Sedimentol.* **2010**, *61*, 177–224.
6. Chen, J.; Zhang, D.D.; Wang, S.; Xiao, T.; Huang, R. Factors controlling tufa deposition in natural waters at waterfall sites. *Sediment. Geol.* **2004**, *166*, 353–366. [[CrossRef](#)]
7. Arenas, C.; Vázquez-Urbez, M.; Auqué, L.; Sancho, C.; Osácar, C.; Pardo, G. Intrinsic and extrinsic controls of spatial and temporal variations in modern fluvial tufa sedimentation: A thirteen-year record from a semi-arid environment. *Sedimentology* **2014**, *61*, 90–132. [[CrossRef](#)]
8. Fouke, B.W. Hot-spring Systems Geobiology: Abiotic and biotic influences on travertine formation at Mammoth Hot Springs, Yellowstone National Park, USA. *Sedimentology* **2011**, *58*, 170–219. [[CrossRef](#)]
9. Di Benedetto, F.; Montegrossi, G.; Minissale, A.; Pardi, L.A.; Romanelli, M.; Tassi, F.; Delgado Huertas, A.; Pampin, E.M.; Vaselli, O.; Borrini, D. Biotic and inorganic control on travertine deposition at Bullicame 3 spring (Viterbo, Italy): A multidisciplinary approach. *Geochim. Cosmochim. Acta* **2011**, *75*, 4441–4455. [[CrossRef](#)]
10. Dupraz, C.; Reid, R.P.; Braissant, O.; Decho, A.W.; Norman, R.S.; Visscher, P.T. Processes of carbonate precipitation in modern microbial mats. *Earth Sci. Rev.* **2009**, *96*, 141–162. [[CrossRef](#)]
11. Zhang, D.D.; Zhang, Y.; Zhu, A.; Cheng, X. Physical Mechanisms of River Waterfall Tufa (Travertine) Formation. *J. Sediment. Res.* **2001**, *71*, 205–216. [[CrossRef](#)]
12. Winsborough, B.M. *Diatoms and Benthic Microbial Carbonates*; Springer: Berlin/Heidelberg, Germany, 2000; pp. 76–83.
13. Sun, S.; Dong, F.; Ehrlich, H.; Zhao, X.; Liu, M.; Dai, Q.; Li, Q.; An, D.; Dong, H. Metabolic influence of psychrophilic diatoms on travertines at the Huanglong Natural Scenic District of China. *Int. J. Environ. Res. Public Health* **2014**, *11*, 13084–13096. [[CrossRef](#)] [[PubMed](#)]
14. Gradzinski, M. Factors controlling growth of modern tufa: Results of a field experiment. *Geol. Soc. Lond. Spec. Publ.* **2010**, *336*, 143–191. [[CrossRef](#)]
15. Merz-Preiß, M.; Riding, R. Cyanobacterial tufa calcification in two freshwater streams: Ambient environment, chemical thresholds and biological processes. *Sediment. Geol.* **1999**, *126*, 103–124. [[CrossRef](#)]

16. Drysdale, R.N.; Taylor, M.P.; Ihlenfeld, C. Factors controlling the chemical evolution of travertine-depositing rivers of the Barkly karst, northern Australia. *Hydrol. Process.* **2002**, *16*, 2941–2962. [[CrossRef](#)]
17. Meldrum, F.C.; Hyde, S.T. Morphological influence of magnesium and organic additives on the precipitation of calcite. *J. Cryst. Growth* **2001**, *231*, 544–558. [[CrossRef](#)]
18. Lebron, I.; Suarez, D.L. Calcite nucleation and precipitation kinetics as affected by dissolved organic matter at 25 °C and pH > 7.5. *Geochim. Cosmochim. Acta* **1996**, *60*, 2765–2776. [[CrossRef](#)]
19. Lin, Y.P.; Singer, P.C. Inhibition of calcite crystal growth by polyphosphates. *Water Res.* **2005**, *39*, 4835–4843. [[CrossRef](#)] [[PubMed](#)]
20. Xu, Y.H.; Tang, Y.; Zhang, C.S.; Wang, J.Y.; Li, B. Contamination assessment of heavy metals in road dusts and soils of the Jiuzhaigou National Scenic Area in Sichuan, China. *J. Mt. Sci.* **2010**, *28*, 288–293. [[CrossRef](#)]
21. Gu, Y.; Du, J.; Ya, T.; Qiao, X.; Bossard, C.; Deng, G.P.; Wahnschafft, R.; Blanc, D.L. Challenges for sustainable tourism at the Jiuzhaigou World Natural Heritage site in western China. *Nat. Resour. Forum* **2013**, *37*, 103–112. [[CrossRef](#)]
22. Florsheim, J.L.; Ustin, S.L.; Tang, Y.; Di, B.; Huang, C.; Qiao, X.; Peng, H.; Zhang, M.; Cai, Y. Basin-scale and travertine dam-scale controls on fluvial travertine, Jiuzhaigou, southwestern China. *Geomorphology* **2013**, *180–181*, 267–280. [[CrossRef](#)]
23. Li, S.; Hu, X.; Tang, Y.; Huang, C.; Xiao, W. Changes in lacustrine environment due to anthropogenic activities over 240 years in Jiuzhaigou National Nature Reserve, southwest China. *Quat. Int.* **2014**, *349*, 367–375. [[CrossRef](#)]
24. Wen, X.Y.; Huang, C.M.; Tang, Y.; Gong-Bo, S.L.; Hu, X.X.; Wang, Z.W. Rare earth elements: A potential proxy for identifying the lacustrine sediment source and soil erosion intensity in karst areas. *J. Soils Sediments* **2014**, *14*, 1693–1702. [[CrossRef](#)]
25. Schwartz, M.W.; Dolanc, C.R.; Gao, H.; Strauss, S.Y.; Schwartz, A.C.; Williams, J.N.; Tang, Y. Forest structure, stand composition, and climate-growth response in montane forests of Jiuzhaigou National Nature Reserve, China. *PLoS ONE* **2013**, *8*, e71559. [[CrossRef](#)] [[PubMed](#)]
26. Li, W.; Ge, X.; Liu, C. Hiking trails and tourism impact assessment in protected area: Jiuzhaigou Biosphere Reserve, China. *Environ. Monit. Assess.* **2005**, *108*, 279–293. [[CrossRef](#)] [[PubMed](#)]
27. Qiao, X.; Tang, Y.; Hu, J.; Zhang, S.; Li, J.; Kota, S.H.; Wu, L.; Gao, H.; Zhang, H.; Ying, Q. Modeling dry and wet deposition of sulfate, nitrate, and ammonium ions in Jiuzhaigou National Nature Reserve, China using a source-oriented CMAQ model: Part I. Base case model results. *Sci. Total Environ.* **2015**, *532*, 831–839. [[CrossRef](#)] [[PubMed](#)]
28. Tang, Y.; Gao, W.; Wang, X.; Ding, S.; An, T.; Xiao, W.; Wong, M.H.; Zhang, C. Variation of arsenic concentration on surfaces of in-service CCA-treated wood planks in a park and its influencing field factors. *Environ. Monit. Assess.* **2015**, *187*, 4214–4225. [[CrossRef](#)] [[PubMed](#)]
29. Gao, L.; Tang, Y.; Bossard, C.; Wang, Y.; Han, Z. Diurnal variation in relative photosynthetic performance of marestalk (*Hippuris vulgaris* Linn.) Across a water temperature gradient using PAM fluorometry in Jiuzhaigou National Nature Reserve, Sichuan Province, China. *J. Mt. Sci.* **2011**, *8*, 794–807. [[CrossRef](#)]
30. Zhang, J.L.; Wang, H.J.; Liu, Z.H.; An, D.J.; Dreybrodt, W. Spatial-temporal variations of travertine deposition rates and their controlling factors in Huanglong Ravine, China—A world’s heritage site. *Appl. Geochem.* **2012**, *27*, 211–222. [[CrossRef](#)]
31. Stumm, W.; Morgan, J.J. *Aquatic Chemistry: Chemical Equilibria and Rates in Natural Waters*; John Wiley & Sons: New York, NY, USA, 1996; Volume 179.
32. Zhang, Z.; Pentecost, A. New and noteworthy bryophytes from the travertines of Guizhou and Sichuan, S. W. China. *J. Bryol.* **2000**, *22*, 66–68.
33. Ouyang, L.; Pan, Y.; Huang, C.; Tang, Y.; Du, J.; Xiao, W. Water quality assessment of benthic diatom communities for water quality in the subalpine karstic lakes of Jiuzhaigou, a world heritage site in China. *J. Mt. Sci.* **2016**, *13*, 1632–1644. [[CrossRef](#)]
34. Liu, Z.; Svensson, U.; Dreybrodt, W.; Yuan, D.; Buhmann, D. Hydrodynamic control of inorganic calcite precipitation in Huanglong Ravine, China: Field measurements and theoretical prediction of deposition rates. *Geochim. Cosmochim. Acta* **1995**, *59*, 3087–3097.
35. Chafetz, H.; Rush, P.F.; Utech, N.M. Microenvironmental controls on mineralogy and habit of CaCO<sub>3</sub> precipitates: An example from an active travertine system. *Sedimentology* **2006**, *38*, 107–126. [[CrossRef](#)]

36. Forbes, M.; Vogwill, R.; Onton, K. A characterisation of the coastal tufa deposits of south-west Western Australia. *Sediment. Geol.* **2010**, *232*, 52–65. [[CrossRef](#)]
37. Pentecost, A. The tufa deposits of the Malham district, north Yorkshire. *Field Stud.* **1981**, *5*, 365–387.
38. Liu, Z.; Zhang, M.; Li, Q.; You, S. Hydrochemical and isotope characteristics of spring water and travertine in the Baishuitai area (SW China) and their meaning for paleoenvironmental reconstruction. *Environ. Geol.* **2003**, *44*, 698–704. [[CrossRef](#)]
39. Pentecost, A.; Viles, H. A Review and Reassessment of Travertine Classification. *Geogr. Phys. Quat.* **1994**, *48*, 305–314. [[CrossRef](#)]
40. Wan, L.; Cao, W.; Hu, F.; Jin, X.; Chen, J.; Gong, B. *Eco-Hydrogeology*; Geology Press: Beijing, China, 2005.
41. Adesuyi, A.; Nnodu, V.; Njoku, K.; Anuoluwapo, J. Nitrate and Phosphate Pollution in Surface Water of Nwaja Creek, Port Harcourt, Niger Delta, Nigeria. *Int. J. Geol. Agric. Environ. Sci.* **2015**, *3*, 13–20.
42. Qiao, X.; Du, J.; Lugli, S.; Ren, J.; Xiao, W.; Chen, P.; Tang, Y. Are climate warming and enhanced atmospheric deposition of sulfur and nitrogen threatening tufa landscapes in Jiuzhaigou National Nature Reserve, Sichuan, China? *Sci. Total Environ.* **2016**, *562*, 724–731. [[CrossRef](#)] [[PubMed](#)]
43. Kazmierczak, K. The role of alkalinity in the evolution of ocean chemistry, organization of living systems, and biocalcification processes. *Prep. Biochem.* **1994**, *7*, 345–355.
44. Yoshimura, K.; Liu, Z.; Cao, J.; Yuan, D.; Inokura, Y.; Noto, M. Deep source CO<sub>2</sub> in natural waters and its role in extensive tufa deposition in the Huanglong Ravines, Sichuan, China. *Geol. Geochem.* **2005**, *205*, 141–153. [[CrossRef](#)]
45. Fouke, B.W.; Farmer, J.D.; Des Marais, D.J.; Pratt, L.; Sturchio, N.C.; Burns, P.C.; Discipulo, M.K. Depositional facies and aqueous-solid geochemistry of travertine-depositing hot springs (Angel Terrace, Mammoth Hot Springs, Yellowstone National Park, U.S.A.). *J. Sediment. Res.* **2000**, *70*, 565–585. [[CrossRef](#)]
46. De Wet, C.B.; Davis, K. Preservation potential of microorganism morphologies in tufas, sinters, and travertines through geologic time. *Palaeobiodivers. Palaeoenviron.* **2010**, *90*, 139–152. [[CrossRef](#)]
47. Arenas, C.; Cabrera, L.; Ramos, E. Sedimentology of tufa facies and continental microbialites from the Palaeogene of Mallorca Island (Spain). *Sediment. Geol.* **2007**, *197*, 1–27. [[CrossRef](#)]
48. Arenas, C.; Pomar, L. Microbial deposits in upper Miocene carbonates, Mallorca, Spain. *Palaeogeogr. Palaeoclim. Palaeoecol.* **2010**, *297*, 465–485. [[CrossRef](#)]
49. Angeli, N.; Cantonati, M.; Spitale, D.; Lange-Bertalot, H. A comparison between diatom assemblages in two groups of carbonate, low-altitude springs with different levels of anthropogenic disturbances. *J. Czech Phycol. Soc.* **2010**, *10*, 115–128. [[CrossRef](#)]
50. Potapova, M.; Charles, D.F. Diatom metrics for monitoring eutrophication in rivers of the United States. *Ecol. Indic.* **2007**, *7*, 48–70. [[CrossRef](#)]
51. Wang, P.; Shen, H.; Xie, P. Can hydrodynamics change phosphorus strategies of diatoms?—Nutrient levels and diatom blooms in lotic and lentic ecosystems. *Microb. Ecol.* **2012**, *63*, 369–382. [[CrossRef](#)] [[PubMed](#)]
52. Urgenson, L.; Schmidt, A.H.; Combs, J.; Harrell, S.; Hinckley, T.; Yang, Q.; Ma, Z.; Yongxian, L.; Hongliang, L.; MacIver, A. Traditional Livelihoods, Conservation and Meadow Ecology in Jiuzhaigou National Park, Sichuan, China. *Hum. Ecol.* **2014**, *42*, 481–491. [[CrossRef](#)] [[PubMed](#)]

